Modeling future glacier mass balance and volume changes using ERA-40 reanalysis and climate models: A sensitivity study at Storglaciären, Sweden

Valentina Radić[1] and Regine Hock[1]

Received 10 November 2005; revised 23 March 2006; accepted 3 April 2006; published 13 July 2006.

[1] Modeling the response of glaciers to future climate change is important for predicting changes in global sea level rise and local water resources. We compute until the year 2100 the mass balance and volume evolution of Storglaciären, a small valley glacier in Sweden, using a temperature index mass balance model. We focus on the sensitivity of results to the choice of climate model and variants of adjusting ERA-40 temperatures to local conditions. ERA-40 temperature and precipitation series from 1961 to 2001 are validated and used both as input to the mass balance model and for statistical downscaling of one regional and six global climate models (GCMs). Future volume projections are computed using area-volume scaling and constant glacier area. ERA-40 data correlate well with observations and capture observed interannual variability of temperature and precipitation. The mass balance model driven by several variants of ERA-40 input performs similarly well regardless of temporal resolution of the input series (daily or monthly). The model explains ~70% of variance of measured mass balance when the input temperatures are reduced by the lapse rate that maximizes model performance. Fitting ERA-40 temperatures to observations close to the glacier does not improve the performance of the model, leading us to conclude that ERA-40 can be used for mass balance modeling independent of meteorological observations. Projected future volume series show a loss of 50–90% of the initial volume by 2100. The differences in volume projections vary by 40% of the initial volume for six different GCMs input to mass balance model, while each volume projection varies by 20% depending on whether volume-area scaling or constant area is used and by 10% depending on details in the mass balance model used. The correction of biases in the seasonal temperature cycle of the GCMs with respect to the ERA-40 data is crucial for deriving realistic volume evolution. Static mass balance sensitivities to temperature and precipitation change in the 21st century are -0.48 m yr^{-1} K^{-1} and 0.025 m yr^{-1} per % increase, respectively.

Citation: Radić, V., and R. Hock (2006), Modeling future glacier mass balance and volume changes using ERA-40 reanalysis and climate models: A sensitivity study at Storglaciären, Sweden, *J. Geophys. Res.*, *111*, F03003, doi:10.1029/2005JF000440.

1. Introduction

[2] Glaciers have generally retreated during the last century with notably accelerated mass losses in recent years [*Dyurgerov and Meier*, 2000; *Meier et al.*, 2003]. Further glacier wastage will have major implications on all spatial scales, ranging from local effects on river runoff [*Hock et al.*, 2005] to global effects through meltwater contribution to sea level rise [e.g., *Church et al.*, 2001; *Arendt et al.*, 2002]. Modeling the response of glaciers to future climate change therefore has major societal implications. Traditionally, glacier models have been forced by meteorological observations in the vicinity of the glaciers [e.g., *Schneeberger et al.*, 2001; *Aðalgeirsdóttir et al.*, 2006], but scarcity of meteorological data in remote glacierized areas poses serious constraints to such an approach and hampers larger-scale glacier modeling.

[3] Climate reanalysis products can be very useful for investigating climatic patterns of largely inaccessible regions, thus circumventing the need for direct meteorological measurements. Reanalyses are derived by processing multidecadal sequences of past meteorological observations using modern data assimilation techniques developed for numerical weather prediction. The result is a dynamically consistent three-dimensional gridded data set that represents the best estimate of the state of the atmosphere at a certain time. Therefore it should be superior to the gridded climatology of the Climate Research Unit (CRU) which is derived from interpolation of observations [*New et al.*, 1999], and has been used in mass balance modeling [*Raper and Braithwaite*, 2006]. Reanalyses products are as yet little exploited in glacier monitoring. *Hanna et al.* [2001], *Reichert et al.* [2001], and *Rasmussen and Conway* [2004]

[1]Department of Physical Geography and Quaternary Geology, Stockholm University, Stockholm, Sweden.

0148-0227/06/2005JF000440

have used NCEP/NCAR reanalysis or the 15-year reanalysis (ERA-15, 1979–1993) by the European Centre for Medium-Range Weather Forecast (ECMWF) to estimate present glacier mass balance, or have used them to downscale the output from global climate models (GCMs) in order to model future mass balance changes. Recently, ECMWF completed the ERA-40 project, which produced a global reanalysis of the state of the atmosphere, land and surface over the period of mid-1957 to mid-2002 [*Simmons and Gibson*, 2000; *Kållberg et al.*, 2004]. This "second-generation" ECMWF reanalysis, ERA-40, opens a new potential in glacier-climate modeling [e.g., *Velicogna et al.*, 2005].

[4] In this study we estimate the mass balance and volume changes of Storglaciären, a small valley glacier in northern Sweden, for the 21st century using climate scenarios derived from one regional climate model (RCM) and six GCMs downscaled by means of ERA-40 data. Storglaciären is chosen as the best case since it is a well investigated glacier with a wealth of available data. Specifically, it has the longest detailed mass balance record in the world [*Holmlund et al.*, 2005]. We use a simple mass balance model based on air temperature and precipitation data and apply volume-area scaling [*Bahr et al.*, 1997] for the volume change computations.

[5] The specific goals are (1) to validate the ERA-40 data in the study area and to explore the potential to use ERA-40 data in mass balance modeling, (2) to investigate the sensitivity of the results to variations in the input of the mass balance model, such as variations caused by using monthly or daily input data, using different calibration periods, and applying different downscaling methods for the ERA-40 data, (3) to investigate the sensitivity of mass balance and volume predictions to the choice of the GCM, and (4) to derive the mass balance sensitivities for the 21st century. Hence this study focuses on sensitivity analyses, addressing uncertainties in the modeling of the response of glaciers to climate change. We present a methodology to use daily or monthly ERA-40 data and statistically downscaled monthly GCM output for glacier predictions which, due to its modest data requirements, may be suitable to predict future glacier wastage on large spatial scales.

2. Study Site

[6] Storglaciären (67.90°N, 18.57°E) has a length of 3 km and an area of approximately 3.1 km^2, ranging from 1130 m to 1720 m asl in altitude. The average and maximum ice thicknesses are 95 m and 250 m, respectively. The glacier is temperate with a perennial cold (<0°C) surface layer in the ablation area reaching up to 60 m in depth [*Pettersson et al.*, 2004]. Storglaciären is located along a strong climate gradient with a maritime climate in the west and a more continental climate toward the east, due to a dominant wind direction from the west and the effect of topography. The glacier has been intensively studied for several decades. Glaciometeorological studies have revealed that the turbulent fluxes contribute on average 40–60% of the energy available for melt [*Hock and Holmgren*, 1996, 2005]. The mean annual air temperature (1965–2003) at Tarfala Research Station (67.92°N, 18.60°E, 1130 m asl) located ~1 km from the glacier is −3.7°C, and summer temperature (June–August) is 5.7°C, while annual precipitation is estimated to amount roughly to 1000 mm. The glacier has retreated considerably since the beginning of 20th century when its front reached the maximum in response to cooling during the 19th century [*Holmlund*, 1987]. The retreat was interrupted by periods of higher winter precipitation in the mid–1970s which translated into a complete halt in the retreat during the 1980s. A period of significantly enhanced winter precipitation between the late 1980s and mid-1990s caused positive mass balances and mass gain but no change in terminus position. Studies of glacier-climate coupling show that the net balance of Storglaciären is well correlated with the summer temperature at the Tarfala Research Station [*Holmlund*, 1987].

3. Data

[7] Our study is based on various data sets including the mass balance record of Storglaciären, daily temperature data from Tarfala Research Station, daily temperature and precipitation data from four additional meteorological stations up to 80 km away from the glacier, daily temperature and precipitation analyses from ERA-40 and a RCM from several grid points close to the glacier for the period 1958–2001 and 1961–2100, respectively, and monthly temperature and precipitation data from the grid point closest to Storglaciären from six GCMs for the period 1961 to 2100. These data sets are briefly described below.

3.1. Mass Balance of Storglaciären

[8] A detailed mass balance program was initiated in 1945 and revised with time. Since 1966 winter mass balance has been computed from snow probings on a regular 100 × 100 m grid and several density pits. Ablation stakes at a density of about 20 per km^2 are used for the summer balance. Winter and summer data have been extrapolated to five topography maps generated at 10 year intervals to yield area-averaged mass balances [*Holmlund et al.*, 2005]. Since 1969, according to available maps, the glacier area change is less than 1%. Mean winter, summer and net balances (in water equivalent) for the period 1945/1946–2003/2004 are +1.43, −1.66, and −0.23 m yr^{-1}, respectively.

3.2. Meteorological Observations

[9] Daily temperature and precipitation data were available from Tarfala Research Station (67.92°N, 18.58°E, 1135 m asl) for the period 1965 to date and from four additional weather stations run by the Swedish Meteorological and Hydrological Institute (SMHI) but for shorter time periods (Figure 1): Ritsem (67.73°N, 17.47°E, 524 m asl, 1981–2002), Riksgränsen (68.43°N, 18.13°E, 508 m asl, 1961–2002), Abisko (68.36°N, 18.82°E, 388 m asl, 1966–2001) and Nikkaluokta (67.85°N, 19.02°E, 468 m asl, 1966–1975).

3.3. Reanalysis Data: ERA-40

[10] The 40-year reanalysis project of the ECMWF, ERA-40, uses the ECMWF numerical weather forecast model to produce gridded analyses of the state of the atmosphere with a 6-hour time interval. Through data assimilation, meteorological observations along with data from satellites and information from a previous model forecast are input into a short-range weather forecast model. This is integrated

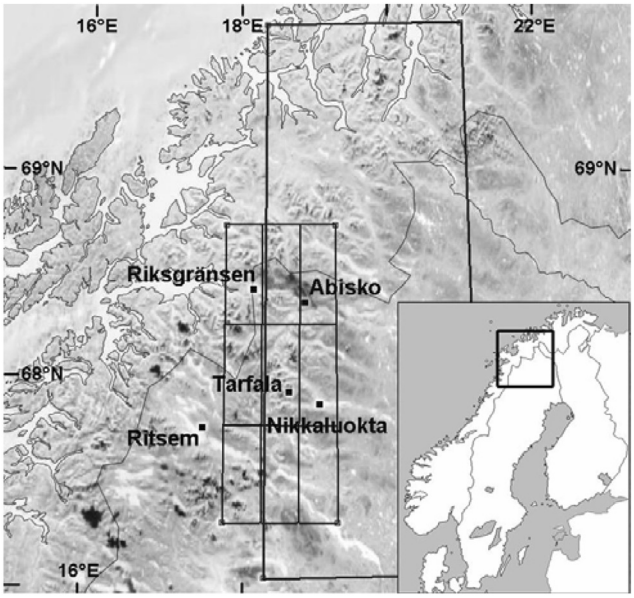

Figure 1. Study area including the meteorological stations used for validation of ERA-40 data. Storglaciären is located ~1 km southwest of Tarfala. Nine grid cells with the resolution of 0.5° × 0.5° (~50 km^2) correspond to ERA-40 gridded data, while the large grid cell for comparison shows the grid cell used from the GCM with highest resolution (ECHAM/OPYC3, 2.8° × 2.8°).

forward and combined with observational data for the corresponding period. ERA-40 is derived for the period of mid-1957 to mid-2002 and it covers the whole globe with spectral resolution T_L159, corresponding to a grid spacing close to 125 km (1.125°) in the horizontal and with sixty levels in the vertical [*Kållberg et al.*, 2004]. Until 1967 almost no observations from Scandinavia were included in the ERA-40 assimilation, which resulted in an underestimation of the observed warming trend over that region for the period 1958–2001. The overall observing system improved at the end of 1978 when more satellite temperature and humidity observations became available to include in the analysis. As a result, the accuracy of medium-range forecasts initiated from the ERA-40 analysis improved from 1979 onward [*Simmons et al.*, 2004]. In comparison with the NCEP/NCAR reanalysis, ERA-40 monthly temperatures show better agreement in trends and variability to the CRU climatology based on observations [*Simmons et al.*, 2004].

[11] We retrieved 6-hourly 2 m air temperature and precipitation ERA-40 data from a bilinearly interpolated grid (0.5° × 0.5°) for the area containing Storglaciären, forming 3 × 3 grid cells with the grid cell containing Storglaciären in the center (Figure 1). The data represent averages over a grid cell. Daily temperature of each grid cell is calculated as the average of the 6-hourly temperature. Daily precipitation is based on the forecasted fields. Since the forecast is affected by spin-up effects, the most reliable technique to derive daily precipitation is to use the 24 h forecasts that are started every 12 hours [*Martin*, 2004]. We subtract the precipitation accumulated in 12 hours for each run from the precipitation accumulated in 24 hours for the same run. Precipitation derived for 00–12 h and 12–24 h time intervals is then summed to provide daily precipitation.

3.4. Regional Climate Model: RCA3

[12] Predictions of temperature and precipitation are derived from the regional climate model RCA3 of the Rossby Centre of the Swedish Meteorological and Hydrological Institute [*Kjellström et al.*, 2005]. It runs with a resolution of about 50 km grid spacing on an area of roughly 5000 × 5000 km^2 with Scandinavia in focus for the time period of 1961–2100. The lateral boundaries are given by output of the General Circulation Model ECHAM4/OPYC3, and runs are forced by A2 and B2 emission scenarios from *Intergovernmental Panel on Climate Change* (*IPCC*) [2001].

[13] We retrieved 3-hour temperature and precipitation data for 1961 to 2100 from the runs with B2 emission scenarios for the grid points covering the study area (66°–70°N, 16°–20°E). The B2 emission scenario represents a modest scenario among the large suite of available emission scenarios. We chose the B2 run since it has widely been used in climate impact studies [e.g., *Oerlemans et al.*, 2005]. Daily data were calculated as the arithmetical averages of 3-hour temperatures and as the sum of 3-hour precipitation values.

3.5. General Circulation Models

[14] Time series of monthly temperature and precipitation as predicted by six GCMs (ECHAM/OPYC3, HADCM3, CSIRO-Mk2, GFDL-R30, CGCM2, CCSR/NIES) were downloaded from the IPCC Data Distribution Centre (http://ipcc-ddc.cru.uea.ac.uk/). As for the RCA data, we use the predictions based on the B2 emission scenario [*IPCC*, 2001]. Downloaded data series span from 1961 to 2100. For each model only the data from the output grid point nearest to Storglaciären was considered in further analysis. More details about the gridded climate data sets are given in Table 1.

4. Methods

[15] We adopt the following overall methodology: First we evaluate the ERA-40 data using meteorological observations, and we derive transfer functions to convert the grid point ERA-40 data to observations. Second, the ERA-40 data are used to calibrate a temperature-index mass balance model where air temperature is related to summer mass balance and precipitation is related to winter mass balance. We compare the performance of nine approaches differing in the temporal resolution of the input data and manipulation of the ERA-40 temperature data. We also investigate the stability of regression coefficients when using different time periods. Third, time series of temperature and precipitation until 2100 are downscaled from RCA3 and the GCMs using ERA-40 data, and then used as input to the mass balance model for projections of mass balance and volume changes of Storglaciären in the coming century. We run eight variants of the calibrated mass balance model with the RCA3-derived climate scenario to study the sensitivity of the mass balance model. The variant with highest performance is then run with climate forcing derived from

Table 1. Gridded Climate Data Sets Used in This Study Including Horizontal Resolution and the Elevation and Coordinates of the Grid Point Closest to Storglaciären

Data Set	Model	Resolution	Elevation, m asl	Coordinates
Reanalysis	ERA-40	0.5° × 0.5°	509	68.50°N 18.00°E
Regional climate model	RCA3	0.5° × 0.5°	990	68.00°N 18.40°E
Global climate model	HADCM3	3.75° × 2.5°	527	67.50°N 18.75°E
Global climate model	CSIRO-Mk2	5.6° × 3.2°	325	68.50°N 16.88°E
Global climate model	GFDL-R30	3.75° × 2.2°	190	68.20°N 18.75°E
Global climate model	CGCM2	3.75° × 3.7°	134	68.65°N 18.75°E
Global climate model	CCSR/NIES	5.6° × 5.5°	22	69.21°N 16.88°E
Global climate model	ECHAM/OPYC3	2.8° × 2.8°	334	68.37°N 19.69°E

six GCMs in order to investigate the sensitivity of results to the choice of the climate model. We also compare the impact of using predictions based upon volume-area scaling versus predictions assuming constant glacier area. Finally, static sensitivities for 21st century are computed from the RCA3 run.

4.1. Validation of Temperature and Precipitation From ERA-40

[16] Linear regression analysis is applied in order to investigate the correlation between the ERA-40 data and the observational data on daily, monthly and seasonal timescales. We use temperature data from Tarfala Research Station (1965–2002) since it is located in the immediate vicinity of Storglaciären. Ritsem's data (1981–2002) are used for validation of precipitation, since year-round precipitation data are not available from Tarfala, and Ritsem's data has been shown to correlate best with Storglaciären's winter balance compared to data from other surrounding stations [*de Woul and Hock*, 2005].

[17] In order to analyze interannual variability of temperature and precipitation without being affected by systematic bias, time series of the temperature and precipitation ratio, R, between two consecutive years are estimated as follows:

$$R = \frac{X(t)}{X(t+1)}, \tag{1}$$

where t is the time index of the year, R equals R_{OBS} (R_{ERA}) when X corresponds to 3-month averaged observational (ERA-40) data. Correlations between R_{OBS} and R_{ERA} are then used as indicators of correlation of interannual variability between ERA-40 and observational data. The function $F(t)$ expressed as:

$$F(t) = \frac{R_{ERA}(t)}{R_{OBS}(t)} \tag{2}$$

indicates high interannual similarity if $F(t)$ values are near unity.

[18] Since the gridded and the measured data refer to different elevations, temperature differences between ERA-40 and the observations from Tarfala station and three additional meteorological stations (Riksgränsen, Abisko and Nikkaluokta; Figure 1) were analyzed in order to adjust ERA-40 temperature to local conditions.

4.2. Mass Balance Model

[19] Melt has been found to correlate well with air temperature [e.g., *Krenke and Khodakov*, 1966; *Braithwaite*, 1984; *Vallon et al.*, 1998] forming the basis for most mass balance models [*Hock*, 2003]. We use a simple degree-day approach following *de Woul and Hock* [2005]:

$$b_s = \alpha_s \sum_{i=t_1}^{t_2} a_i T_i + \beta_s, \quad \begin{cases} a_i = 1, T_i > 0 \\ a_i = 0, T_i \le 0 \end{cases} \tag{3}$$

$$b_w = \alpha_w \sum_{i=t_1}^{t_2} a_i P_i + \beta_w, \quad \begin{cases} a_i = 1, T_i < 0 \\ a_i = 0, T_i \ge 0 \end{cases} \tag{4}$$

where α and β are the coefficients derived from linear regression between measured summer mass balances (b_s) and positive degree-day sums ($\Sigma a_i T_i$) over the entire mass balance year and between measured winter mass balances (b_w) and annual sums of daily/monthly precipitation ($\Sigma a_i P_i$) with negative air temperatures. The mass balance year is defined from 1 October (t_1) to 31 September (t_2). The model needs calibration based on seasonal mass balance data, thus hampering direct transferability to other glaciers.

[20] We aim to show if and how much ERA-40 needs to be adjusted (downscaled) before being used in the model. Therefore the model performance, i.e., the percentage of the explained variance of measured mass balance by the modeled one, is tested according to nine variants of the model input. Variants differ in the temporal resolution of the input data (seasonal, daily or monthly averages) and in the method by which ERA-40 temperatures are adjusted prior to model input. In methods 1–3 T_i is taken from ERA-40 without any adjustments, while in methods 4–9 temperatures are adjusted by different types of lapse rates to represent local conditions. The following input variants are used.

[21] 1. $\Sigma a_i T_i$ is equal to the sum of mean June, July and August temperatures ($T_{Jun} + T_{Jul} + T_{Aug}$), while $\Sigma a_i P_i$ is the sum of precipitation from all months except June, July and August.

[22] 2. T_i is monthly mean temperature and P_i is monthly precipitation sum.

[23] 3. T_i is daily temperature and P_i is daily precipitation sum.

[24] 4. T_i is daily temperature which is adjusted in two steps: first by adjusting ERA-40 temperatures using the monthly variable lapse rate derived from validation of ERA-40 with Tarfala temperature data. By this ERA-40 temperatures are fit to the observations. The second step is further reduction of the temperature by the lapse rate (between

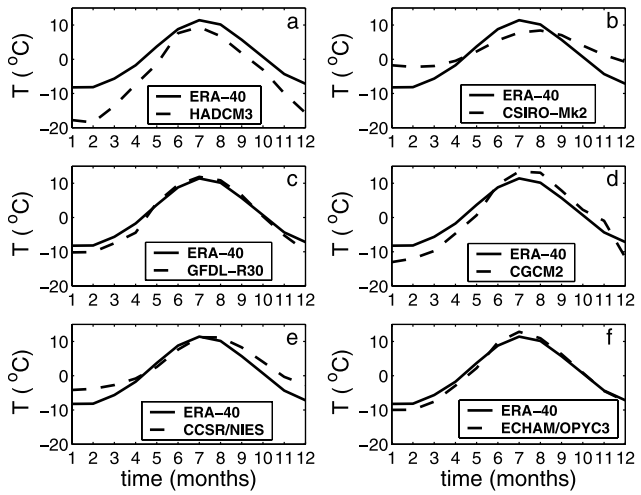

Figure 2. Temperature seasonal cycles averaged over 1961–2001 from ERA-40 and six GCMs, compared before the statistical downscaling is applied to the output of GCMs.

Tarfala elevation and Storglaciären's equilibrium line altitude = 1468 m) that maximizes correlation between degree-day sums ($\Sigma a_i T_i$) and b_s. P_i is daily precipitation sum.

[25] 5. Method is as in 4, but T_i and P_i are monthly data.

[26] 6. T_i is daily temperature lowered by the lapse rate that maximizes correlation between degree-day sums ($\Sigma a_i T_i$) and b_s. Hence observational data are not needed. P_i is daily precipitation sum.

[27] 7. Method is as in 6, but T_i and P_i are monthly data.

[28] 8. T_i is monthly temperature lowered by the average lapse rate derived from the temperature and altitude difference between ERA-40 and four meteorological stations. P_i is monthly precipitation sum.

[29] 9. T_i is synthetic temperature data derived from the monthly data from 5 applying a normal distribution of daily temperatures from 4. The normal distribution is derived for each month of each year and the method is used only for calibration of summer mass balance. Winter mass balance is not modeled for this case.

[30] A set of coefficients α and β was determined by regression analysis for each of the methods. To investigate the stability of coefficients with time, regression analysis was performed for three different time periods: 1965/1966–1980/1981, 1980/1981–2001/2002, and 1965/1966–2000/2001. Net mass balance is derived as the sum of the winter mass balance and (negative) summer mass balance.

4.3. Future Runs of Mass Balance Model

4.3.1. Climate Forcing

[31] Direct use of meteorological output from climate models is currently not applicable for impact studies, as climate models are unable to represent local subgrid-scale features and dynamics [*Giorgi et al.*, 2001] which leads to biases in both temperature and precipitation. Since the degree-day model is particularly sensitive to the seasonal distribution of temperature, such differences will strongly affect the mass balance simulations. Also, the direct use of coarse GCM grid points naturally results in a poor representation of the local climate, especially for precipitation, which is highly dependent on the local orographic conditions. Therefore downscaling techniques need to be applied to the climate model output [*Wilby et al.*, 1998; *Giorgi et al.*, 2001]. Downscaling methods generally use observations as a reference climate [*Salathé*, 2005]. We use ERA-40 because these data are the input to the mass balance model. We apply a simple statistical downscaling method, referred to as 'local scaling' [*Widmann et al.*, 2003; *Salathé*, 2005], which for temperature can be thought as a lapse rate correction due to elevation difference of the local grid point relative to the climate model grid. Downscaled series were produced for RCA3 and each GCM for the period 2001 to 2100 by correcting the monthly climate model output series by the averaged difference over a baseline period prior to 2001 between climate model and ERA-40 for each month. Hence the average seasonal cycle from ERA-40 is used as a reference by which the seasonal cycle from the climate model is 'corrected'. Future temperature time series (T_i) were calculated by

$$T_i(t) = T_{i,c}(t) + \left(\overline{T_{i,ERA}} - \overline{T_{i,c}}\right), \qquad i = 1, \ldots, 12 \tag{5}$$

where $T_{i,c}$ is monthly temperature for the ith month from the climate model output from t = 2001 to 2100, $\overline{T_{i,c}}$ and $\overline{T_{i,ERA}}$ are mean temperature from climate model and ERA-40, respectively, for the ith month averaged over a chosen baseline period. Five different baseline periods are chosen for comparison: 1961–2001, 1971–2001, 1981–2001, 1991–2001 and 2000–2001.

[32] As an example, Figure 2 shows the seasonal cycles for ERA-40 temperatures averaged over the 1961–2001 period compared with those modeled by the six GCMs. Although overall patterns are reproduced well, some models have strong seasonal biases. CSIRO and CCSR/NIES have the temperature maximum shifted by one month combined with subdued seasonality, probably since the grid cell used contains large ocean percentage due to coarse horizontal resolution.

[33] For precipitation, the local scaling method simply multiplies the large-scale simulated precipitation at each local grid point by a seasonal scale factor [*Widmann et al.*, 2003]. Since changes in precipitation over the year show no obvious seasonal cycle but a more random distribution, we scale precipitation equally throughout the year. Thus the future series $P_i(t)$ is generated by

$$P_i(t) = P_{i,c}(t)\frac{\overline{P_{ERA}}}{\overline{P_c}}, \qquad i = 1, \ldots, 12 \tag{6}$$

where $P_{i,c}$ is monthly precipitation sum from the climate model from t = 2001 to 2100, $\overline{P_c}$ and $\overline{P_{ERA}}$ are mean precipitation from the climate model and ERA-40, respectively, averaged over the baseline period. Climate models tend to underestimate large amounts of precipitation and overestimate small amounts [*Xu*, 1999]. This is also a characteristic of ERA-40 precipitation when compared to observations from Ritsem station (Figure 3). However, ERA-40 captures well the temporal variability, which is more crucial than absolute amounts for the type of mass balance model chosen (equation (4)). Figure 4 illustrates the annual time series of temperature and precipitation derived

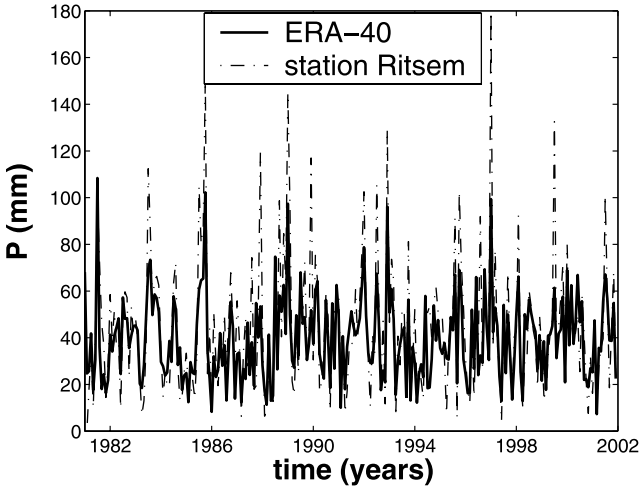

Figure 3. Monthly sums of precipitation from ERA-40 reanalysis and Ritsem.

from downscaling the RCA3 model with different baseline periods. Since the differences in the series resulting from the baseline periods 1961–2001, 1971–2001, 1981–2001 and 1991–2001 are too small to be distinguished in Figure 4, only one of these series is presented while the series derived from 2-year baseline period 2000–2001 shows notable differences.

4.3.2. Volume Changes

[34] In response to prolonged mass balance changes, glacier area and volume will change. These changes may be approximated by volume-area scaling [*Bahr et al.*, 1997; *Van de Wal and Wild*, 2001]. Glacier volume change, ΔV, is estimated by

$$\Delta V(t) = b_n(t)A(t), \tag{7}$$

where b_n is the modeled future annual net mass balance and A is the area of the glacier. Volume V is related to area A by the empirical relation:

$$V(t) = k[A(t)]^{\gamma}, \tag{8}$$

where $\gamma = 1.375$ was obtained by *Bahr et al.* [1997] using theoretical considerations and the constant $k = 0.0633\ \mathrm{km}^{3-2\gamma}$ is derived from Storglaciären's initial volume $V(t = 2001) = 0.3\ \mathrm{km}^3$ and the initial area $A(t = 2001) = 3.1\ \mathrm{km}^2$. After each mass balance year a new volume is computed from which a new glacier area is derived. For comparison, we also perform runs with glacier area kept constant.

4.3.3. Static Mass Balance Sensitivity

[35] Modeled future mass balances are used to estimate static mass balance sensitivities due to temperature (db/dT) and precipitation (db/dP) changes. The concept of mass balance sensitivity [e.g., *Braithwaite et al.*, 2002] has been widely used in predicting glacier changes [*Gregory and Oerlemans*, 1998; *Oerlemans et al.*, 1998, 2005]. We derive static mass balance sensitivities in the 21st century by calculating time series of db/dT and db/dP based on the difference between 20-year running averages of mass balances, temperature and precipitation, and corresponding averages over a fixed 20-year reference period (2001–2020):

$$\frac{db}{dT} = \frac{\sum_{t=t_o+1}^{t_0+20} b_n(t) - \sum_{t=2001}^{2020} b_n(t)}{\sum_{t=t_0+1}^{t_0+20} T(t) - \sum_{t=2001}^{2020} T(t)}, \tag{9}$$

$$\frac{db}{dP} = \frac{\frac{1}{20}\sum_{t=t_o+1}^{t_0+20} b_n(t) - \frac{1}{20}\sum_{t=2001}^{2020} b_n(t)}{\left(\frac{\sum_{t=t_0+1}^{t_0+1} P(t)}{\sum_{t=2001}^{2020} P(t)} - 1\right)100}, \tag{10}$$

with $t_0 = 2001, \ldots, 2080$, where mass balance, temperature and sums of precipitation are averaged for consecutive 20-year intervals starting from 2001.

[36] As mass balance sensitivity to temperature change (db/dT) is not independent of precipitation change, and vice versa, additional estimates of sensitivities are calculated to separate both climate signals in the modeled mass balance change. This is done by calculating db/dT from mass balance predictions where climate model temperature predictions are included but the precipitation is held constant in time, i.e., equal to monthly averaged ERA-40 precipitation over the period 1961–2001. Analogously, db/dP is computed from a model run including climate model precipitation predictions, while holding temperature steady, i.e., the seasonal cycle is assumed equal to the averaged cycle from ERA-40 over the period 1961–2001.

[37] In contrast to dynamic sensitivities, static sensitivities neglect time-dependent geometry changes and other dynamic and non-linear effects. Although glacier area changes are computed (equation (8)), this has no bearing on the modeled mass balance according to equations (3) and (4). Hence sensitivities according to equations (9) and (10)

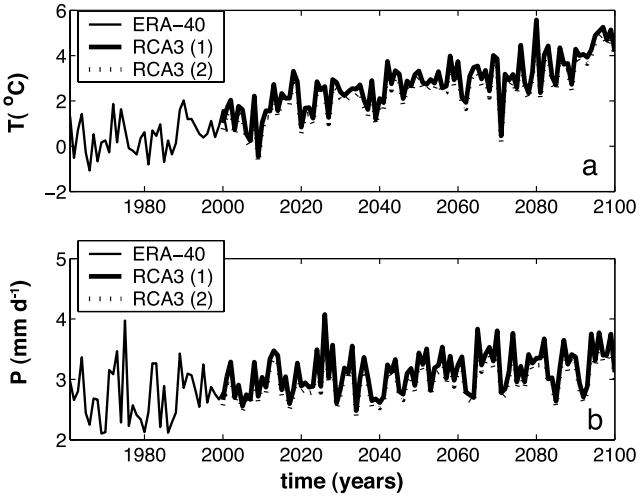

Figure 4. Annual time series of (a) temperature and (b) precipitation, derived from downscaling RCA3 output using two different baseline periods: (1) 41-year period, 1961–2001, and (2) 2-year period, 2000–2001.

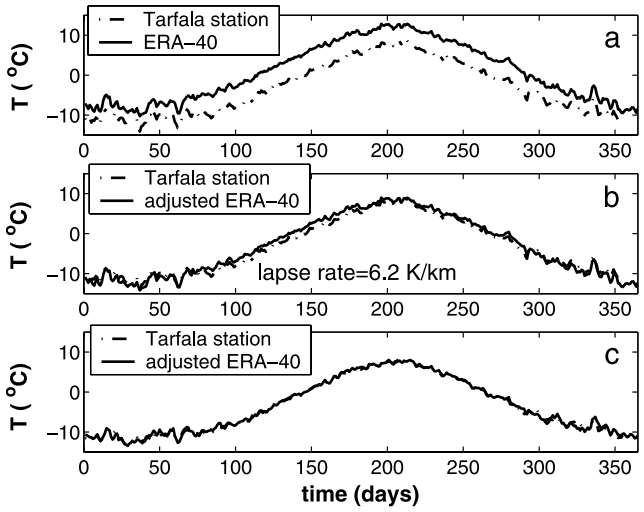

Figure 5. Daily air temperatures averaged over the period 1965–2001 from ERA-40 and Tarfala: (a) without adjustment in ERA-40 data, (b) ERA-40 temperatures lowered by constant lapse rate that yields best agreement with the observations, and (c) ERA-40 temperatures lowered by monthly variable lapse rates (crosses in Figure 6).

are static rather than dynamic. In addition, the mass balance model was calibrated for a period of roughly constant glacier area. Therefore the mass balance record and the derived regression coefficients in the mass balance model reflect climate forcing but neglect the effect of area changes [*Elsberg et al.*, 2001; *Harrison et al.*, 2005].

5. Results and Discussion

5.1. Validation of ERA-40 Temperature

[38] Daily, monthly and annual ERA-40 temperature data of all nine grid points correlate well with the corresponding Tarfala data, yielding $r^2 > 0.8$ for all cases. The data from the grid point northwest from the central grid point shows the highest correlation for daily ($r^2 = 0.927$), monthly ($r^2 = 0.980$) and annual averages ($r^2 = 0.872$), and were thus used in further analysis. R_{ERA} (equation (1)) explains more than 70% of the variance in R_{OBS}, and $F(t)$ (equation (2)) ranged between 0.7 and 1.4, indicating that observed seasonal variability is well represented by ERA-40. Averaged over the period 1965–2001, daily ERA-40 temperatures are systematically higher than the observations, which is partially due to the 626 m difference in elevation between the grid cell and the weather station (Figure 5a). Shifting the ERA-40 series according to an average lapse rate of -0.0062 K m^{-1} yields best agreement with the measurements, although seasonally variable biases are evident (Figure 5b). Such derived 'statistical lapse rates' include temperature variations with elevation, horizontal gradients and model bias. Figure 6 shows the monthly lapse rates that when applied to the ERA-40 yield the best agreement between ERA-40 and observations (Figure 5c). A distinct seasonal cycle is evident; the ERA-40 temperatures require larger reduction with altitude in summer than in winter in order to coincide with the measurements. It must, however, be borne in mind that the seasonal cycle may be due to seasonal variations in both lapse rates and in model bias. The average lapse rate derived from ERA-40 data and annual data from four weather stations amounts -0.0037 K m^{-1} ($r^2 = 0.76$) and is applied in the mass balance model with method 9.

5.2. Validation of ERA-40 Precipitation

[39] Regressing daily, monthly and annual precipitation from ERA-40 (all nine grid points) against corresponding data from Ritsem yields the highest correlation for the grid point west from the central grid point with $r_d^2 = 0.381$, $r_m^2 = 0.670$ and $r_a^2 = 0.563$, respectively. Analysis of seasonal averages revealed that correlation was better in autumn (September, October, November (SON)) and winter (December, January and February (DJF)) than in the remaining seasons ($r_{DJF}^2 = 0.807$, $r_{MAM}^2 = 0.748$, $r_{JJA}^2 = 0.601$, $r_{SON}^2 = 0.882$). As expected, these correlations are lower than those for temperature. When analyzing interannual variability, the highest correlation between R_{OBS} and R_{ERA} was obtained for the winter season ($r_{DJF}^2 = 0.830$, $0.8 < F(t) < 1.3$) and the lowest for the summer season ($r_{JJA}^2 = 0.484$, $0.6 < F(t) < 1.6$). On the basis of high correlation for interannual variability we conclude that ERA-40 can be used as a reference for downscaling precipitation (equation (6)).

[40] Generally speaking, our analysis above suggests that ERA-40 temperature and precipitation captures measured seasonal and interannual variability sufficiently well to be used as input for mass balance modeling of Storglaciären.

5.3. Calibration of the Mass Balance Model

[41] Table 2 presents the results of the regression analysis between measured and modeled mass balances, as produced by the nine (1–9) variants of the input to the mass balance model. In most cases correlation is higher for the summer than the winter balance, with r^2 ranging from 0.49 to 0.80 for b_s and 0.28 to 0.73 for b_w. The highest correlations are comparable and even slightly higher than those derived for Storglaciären from model 6 using measured data from Ritsem ($r^2(b_s) = 0.87$, $r^2(b_w) = 0.65$ [*de Woul and Hock*, 2005]).

[42] The most sophisticated method 4, which fits the ERA-40 temperatures to the observed Tarfala temperatures before adjusting it further to the glacier site, does not yield the highest correlation. In fact, all methods except 2 and 3 tend to produce very similar correlations regardless of the

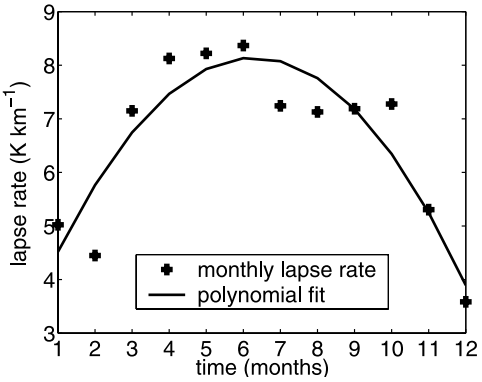

Figure 6. Monthly lapse rates (in absolute values) derived from ERA-40 and Tarfala station temperatures averaged over the period 1965–2001. The line shows a polynomial fit.

Table 2. Explained Variance (r^2) Between the Measured Summer Mass Balances, b_s, and Positive Degree-Day Sums, $\Sigma a_i T_i$, and Between Measured Winter Mass Balances, b_w, and Annual Snow Precipitation, $\Sigma a_i P_i$, as Produced by the Nine Variants of the Input to the Mass Balance Model and for Three Different Calibration Periods[a]

	1965/1966–1980/1981		1980/1981–2000/2001		1965/1966–2000/2001	
Method	b_s	b_w	b_s	b_w	b_s	b_w
1 (m)	0.640	0.657	0.636	0.650	0.642	0.651
2 (m)	0.549	0.462	0.747	0.534	0.566	0.501
3 (d)	0.541	0.405	0.623	0.395	0.503	0.393
4 (d)	0.663	0.676	0.765	0.582	**0.681**	0.634
5 (m)	0.605	0.611	0.776	**0.705**	0.650	0.646
6 (d)	**0.678**	0.634	0.777	0.654	0.679	0.647
7 (m)	0.621	**0.732**	**0.794**	0.640	0.650	**0.653**
8 (d)	0.579	0.400	0.790	0.652	0.631	0.546
9 (m)	0.648		0.751		0.625	

[a]See text for explanation. Letters in parentheses correspond to daily (d) or monthly (m) meteorological input of temperature and precipitation. Highest r^2 for each calibration period are bold.

temperature adjustment to local conditions or whether daily or monthly data are used as input. This aspect is encouraging for use of GCM data for mass balance predictions, since GCM data tend to be most easily accessible with monthly resolution rather than daily. Methods 2 and 3, which exclude any temperature adjustment, yield lower correlation compared with the other methods, emphasizing the importance of adjusting temperature to maximize the correlation between degree-day sums ($\Sigma a_i T_i$) and b_s. This may be considered as a way of tuning the model to achieve the best representation of observed mass balances. However, the tuning is not purely mathematical, because the reduction of temperature in order to achieve better representation of mass balance includes the better representation of temperature at the elevation of the glacier and the locally colder air temperature above the melting glacier surface due to surface cooling [*Braithwaite et al.*, 2002]. Correlations from method 1, which also excludes any temperature adjustment, yield correlations that are similar to methods 4–9 probably because only months with high probability for positive temperatures are included for the summer balance, while the spring and fall periods with temperatures closer to freezing point (thus more sensitive to a temperature bias) are excluded. Adjusting ERA-40 temperatures according to a priori determined lapse rates derived from meteorological observations (methods 4 and 5) does not improve the performance of the model when compared to the methods 6 and 7 which do not require any temperature observations. The latter methods apply a lapse rate (≈ -0.004 K m^{-1}) derived from tuning the mass balance model. This is surprising considering the bias in ERA-40 temperatures (Figure 5a), but also encouraging for ERA-40 driven mass balance modeling in areas where meteorological measurements are not available.

[43] Correlations, especially for summer mass balance, tend to be higher for the calibration period 1980/1981–2000/2001 compared to the preceding period or the total 35-year period. This may be attributed to improved quality in the ERA-40 after the more extensive inclusion of satellite data since 1979. Figure 7 illustrates the measured and modeled b_s, b_w and b_n derived using method 7 for the period 1980/1981–2000/2001. Maximum deviation from the measured b_n is ±0.66 m yr^{-1}, which is equivalent to an error of 0.002 km^3 in the estimation of ΔV. This should be kept in mind when considering calculations of future volume changes in the following section.

5.4. Mass Balance and Volume Projections Until 2100

5.4.1. Sensitivity to Mass Balance Model Input

[44] Volume evolution of Storglaciären as predicted by mass balance modeling with eight methods (1–8) and climate forcing derived from RCA3 model from 2001 to 2100 are presented in Figure 8a. All model variants, except the model using method 1, predict a decrease in initial volume by approximately 30% by 2050 and 60% by 2100. This is due to progressively more negative mass balance, especially after 2040, when b_n becomes consistently negative. Method 1 is an outlier because it calculates melt only in 3 summer months (JJA) while the snow accumulation is equal to all precipitation during the rest of the year. It is therefore unable to capture the prolongation of the melt season associated with future warming and increased probability of precipitation falling as rain from September to May. Albeit achieving comparable correlation coefficients during the calibration period, method 1 is not suitable for climate change impact studies. Method 3 produces the largest mass loss because it uses ERA-40 temperatures without any lapse rate adjustment and therefore estimates more days with positive temperatures over the year and hence more ablation. The differences of modeled volume change by 2100 derived from all methods, excluding methods 1 and 3, are within a range of 10% of initial volume.

[45] Our projection of 30% loss of volume by the middle of the 21st century closely coincides with the loss projected for Storglaciären by a distributed melt model combined with a three-dimensional ice flow model driven by ECHAM4 [*Schneeberger et al.*, 2001]. A one-dimensional ice flow

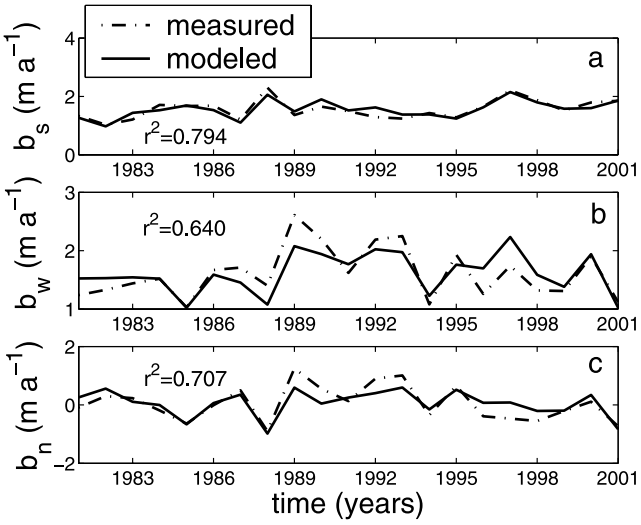

Figure 7. Measured and modeled (a) summer mass balance, b_s, (b) winter mass balance, b_w, and (c) net mass balance, b_n. Modeled mass balance is based on method 7 of the mass balance model and forced by ERA-40 data using the calibration period 1980/1981–2000/2001.

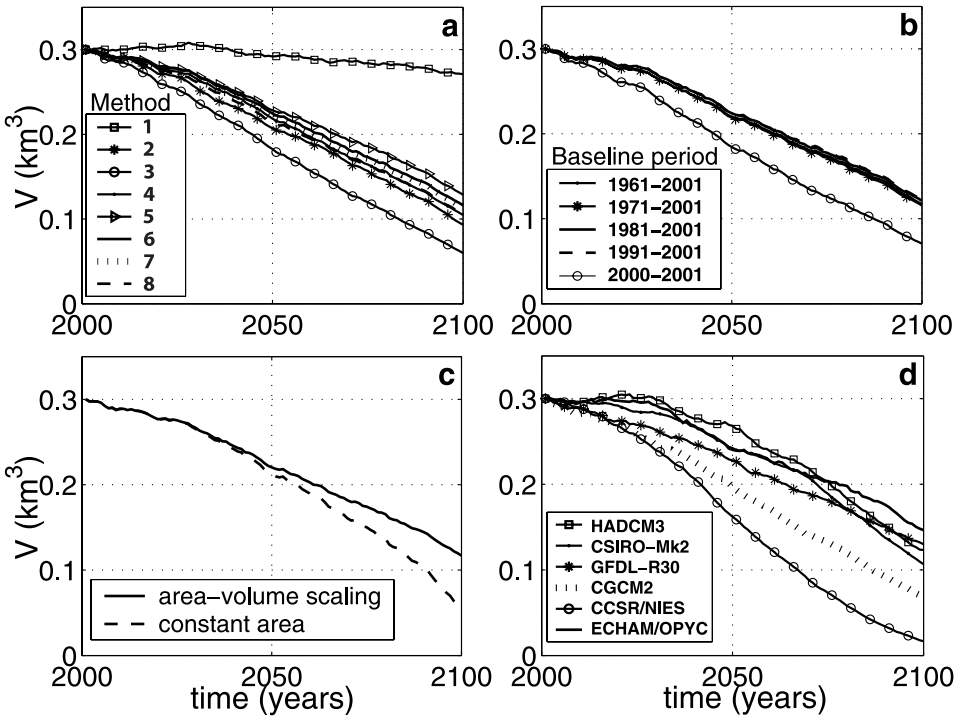

Figure 8. Volume projections for Storglaciären in the 21st century derived from (a) eight methods (1–8) of the mass balance model and RCA3 output downscaled with ERA-40 reference climate for the baseline period 1961–2001, (b) method 7 applied on the RCA3 output downscaled by use of five different baseline periods, (c) method 7 applied on the RCA3, downscaled using the 1961–2001 baseline period and with volume-area scaling and constant area, and (d) method 7 applied on the six GCMs which are downscaled using 1961–2001 baseline period. In all projections, unless noted differently, the volume is derived from volume-area scaling.

model driven by hypothetical warming of 0.02 K per year without change in precipitation projected 20% volume loss by 2050 and 80% loss by 2100 [*Oerlemans et al.*, 1998].

5.4.2. Sensitivity to Choice of Reference Climate

[46] The effect of the choice of the baseline period in generating the future climate time series on the volume evolution is illustrated in Figure 8b which shows the volume evolution estimated by the model with method 7 when the five baseline periods are applied to downscale the RCA3. All volume curves, except for the one forced by the climate series derived from the 2000–2001 baseline, are within a range of 3% of initial volume. This is smaller than the difference caused by the choice of the method for the mass balance model. The outlier is explained by lower future sums of precipitation compared to the sums from other baselines (Figure 4b), which is immediately reflected in reduced winter mass balance and therefore in enhanced loss of mass. It is obvious that the baseline needs to be properly chosen and include a sufficient number of years to subdue the effect of interannual variability. In our case the model is insensitive to the choice of any of the >10 years long baseline periods used.

5.4.3. Sensitivity to the Glacier Area Assumptions

[47] Figure 8c presents the volume change derived from the mass balance model (method 7) with volume-area scaling and with constant area in the equation (7). Until the middle of the 21st century there is no substantial difference between the two curves. Thereafter the volume decrease becomes considerably overestimated (by 20% at the end of 2100) if the area reduction is not considered. Results must be considered as rough estimates since feedback between mass balance and area-elevation distribution is neglected (i.e., mass balance becomes less negative as area is removed from low-lying high-ablation altitudes). The larger volume loss when the glacier area is kept constant is a mathematical consequence of the use of equation (8) when b_n becomes consistently negative.

5.4.4. Sensitivity to Choice of Climate Model

[48] In order to investigate the sensitivity of mass balance and volume predictions to the choice of the GCM, the mass balance model (method 7) is forced by downscaled temperature and precipitation from six GCMs (Figure 8d). Table 3 contains the trends in temperature and precipitation for annual, winter (DJF) and summer (JJA) means.

[49] All models predict volume losses between 50% (ECHAM) to 90% (CCSR) of the initial value. This is a direct consequence of warming trends in the range of 2.3 to 4.9 K per century, which is more evident in the winter than in the summer season for most of the models. Positive trends in precipitation contain relative errors of more than 100% in the estimates (Table 3) which make the trends insignificant. Even if the trend was real, the increase in the range of 57 to 212 mm yr^{-1} per century cannot compensate the increased ablation due to the warming.

[50] The CCSR model predicts the largest mass loss due to its extreme warming trend. CGCM2, although showing

Table 3. Annual, Winter (DJF), and Summer (JJA) Trends in the Climate Models for the Grid Point Nearest to Storglaciären[a]

	Trend					
	Annual		Winter (DJF)		Summer (JJA)	
Model	T	P	T	P	T	P
HADCM3	3.24 ± 0.34	57 ± 41	2.77 ± 0.85	34 ± 21	2.72 ± 0.38	49 ± 20
CSIRO-Mk2	3.11 ± 0.18	136 ± 36	2.90 ± 0.32	44 ± 19	3.02 ± 0.17	10 ± 18
GFDL-R30	2.31 ± 0.37	76 ± 43	2.97 ± 0.87	14 ± 17	1.45 ± 0.40	8 ± 29
CGCM2	2.67 ± 0.35	44 ± 45	2.48 ± 0.87	23 ± 20	1.95 ± 0.28	64 ± 26
CCSR/NIES	4.87 ± 0.20	199 ± 59	5.04 ± 0.36	17 ± 21	4.56 ± 0.25	53 ± 35
ECHAM/OPYC3	3.25 ± 0.31	212 ± 52	4.62 ± 0.62	92 ± 23	1.97 ± 0.50	7 ± 24
RCA3	2.94 ± 0.26	143 ± 38	4.37 ± 0.61	64 ± 17	2.28 ± 0.31	2 ± 22

[a]Temperature trends (T) are in K per century, and precipitation trends (P) are in mm yr^{-1} per century, while the uncertainties are based on the error from the least squares method by which the slope of the trend is determined.

trends comparable with other models, predicts smaller loss of volume than CCSR but larger loss in comparison with the other models. This is due to a sudden shift to higher annual temperatures in the period 2001–2010 and higher maximum temperatures in the interannual variations after 2060 while lacking any trend in precipitation. HADCM3, due to its higher-precipitation and low-temperature trend from 2001 to 2020, predicts a small growth of volume in that period. Afterward the volume decreases due to an increase in temperature. GFDL-R30 follows the volume evolution as in CGCM and CCSR until 2020 when it starts to predict lower mass loss (by 50% at the end of 2100) probably caused by lower slope in temperature trend and, in general, lower minimum temperatures in the interannual variability. ECHAM maintains almost the same volume evolution as CSIRO until 2070 when it shifts to the smaller loss of volume because it projects higher sums of precipitation.

[51] An analysis of the differences in temperature and precipitation trends and interannual variations predicted by the GCMs shows how the differences are highly reflected in the modeled future mass balance. The range of volume change by the end of 2100 is within 40% of the initial volume. This is the largest range in total sensitivity in this study.

[52] One additional test is performed to show the importance of the downscaling method applied on the GCMs: if the future temperature series are corrected with long-term annually averaged temperature instead of monthly averages ($\overline{T_{i,c}}$, $\overline{T_{i,ERA}}$) over the baseline period, as in equation (5), the mass balance model produces the volume changes presented in Figure 9. Results differ considerably from the ones based on monthly averages (Figure 8d), especially for the GCMs with markedly different seasonal cycles compared to the ERA-40 data (Figure 2). Most notably, CSIRO produces a strong volume increase by 2100 despite a significant warming trend. This is caused by a seasonal temperature cycle with too low amplitude causing underestimation of summer temperatures and ablation.

5.4.5. Static Mass Balance Sensitivity

[53] Running 20-year relative changes of net mass balance (*db*), temperature (*dT*) and precipitation (*dP*) with respect to the reference period 2001–2020 are presented in Figure 10. Mass balance is obtained from method 7 of the mass balance model with the climate input from RCA3 downscaled with the baseline period 1961–2001. Temperature change shows constant increase due to a linear warming trend, while % precipitation change shows increase with a secondary minimum at the end of the 2020s. Mass balance changes gradually decrease toward more negative values.

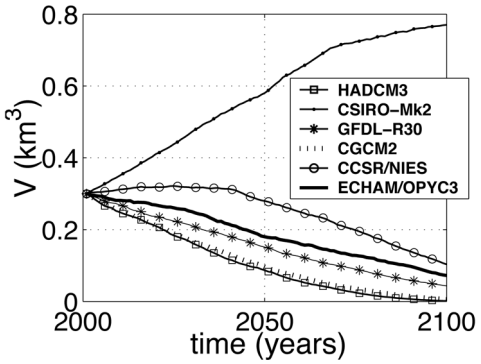

Figure 9. Volume projections for Storglaciären in the 21st century, derived from method 7 of the mass balance model and forced by output from six GCMs. The temperature bias between GCM and ERA-40 is corrected for by the averaged difference over the baseline period 1961–2001 instead of using seasonally variable values.

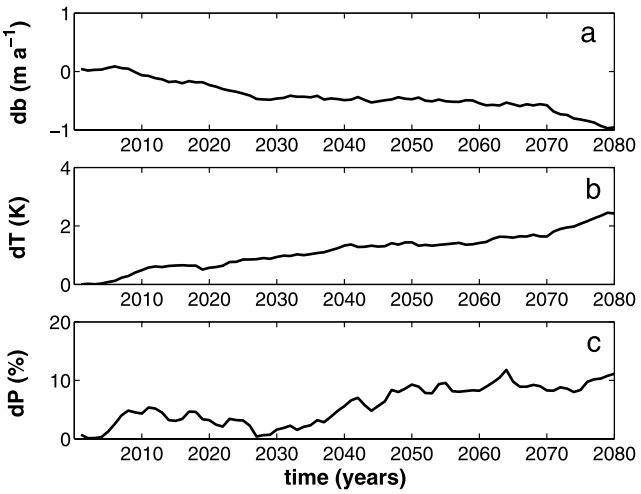

Figure 10. Running 20-year relative changes of (a) net mass balance, *db*, (b) air temperature, *dT*, and (c) precipitation, *dP*, with respect to the reference period 2001–2020.

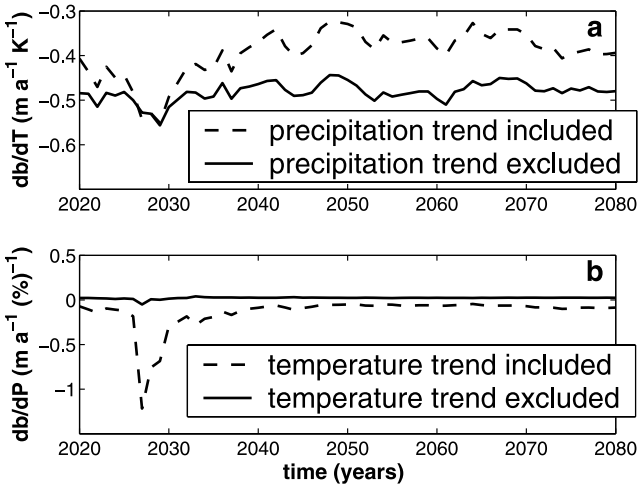

Figure 11. Static mass balance sensitivity due to (a) temperature change, db/dT, and (b) precipitation change, db/dP, calculated from the equations (9) and (10).

[54] The static mass balance sensitivity due to temperature (db/dT) and precipitation (db/dP) change is presented in Figure 11. Sensitivity to temperature, excluding any precipitation trend, varies around the mean value of -0.48 m yr^{-1} K^{-1} with a standard deviation of 0.002 m yr^{-1} K^{-1}. The mean value agrees well with -0.46 m yr^{-1} K^{-1} derived from a model forced by observational data [*de Woul and Hock*, 2005] where a hypothetical increase of 1 K was applied. Also, the result agrees well with -0.48 m yr^{-1} K^{-1} calculated by the degree-day method and local data for Storglaciären [*Braithwaite and Zhang*, 1999]. Sensitivity to precipitation excluding any temperature trend, gives almost a constant value in time: 0.025 m yr^{-1} per 1% increase in precipitation. The negative peak occurring around 2030 is due to the drop in dP (Figure 10). Derived db/dP is slightly higher than the 0.015 m yr^{-1} per 1% increase in precipitation obtained by *de Woul and Hock* [2005].

[55] The results show no substantial variation in static mass balance sensitivity. However, the sensitivity to climate forcing is partly incorporated in the correlation coefficients of the mass balance model, which are kept temporally constant in future projections. Therefore the static sensitivities reflect the linearity of the model and no substantial changes in time are effected given the model assumptions.

6. Conclusions

[56] We have used ERA-40 in the calibration of a simple mass balance model and for downscaling climate models in order to estimate future volume changes of Storglaciären. Our main findings are as follows.

[57] 1. Validation of ERA-40 in the Storglaciären's region showed that ERA-40 temperature explains more than 80% of the variance of observed daily, monthly and annual temperatures at Tarfala Station and that interannual variability is captured well. Precipitation from ERA-40 explains, on average, 50% of the variance of observed precipitation sums at Ritsem station and interannual variability is captured sufficiently well for use in the mass balance modeling.

[58] 2. A mass balance model driven by nine variants of ERA-40 input performs similarly well regardless of temporal resolution of the input data (daily or monthly averages). The model explains 70% of the variance of measured mass balance when the ERA-40 temperatures are reduced by the optimized (tuned) lapse rate between grid point elevation and glacier's ELA. Fitting ERA-40 temperatures to observations does not improve the performance of the model. Hence, in this case ERA-40 can be used for mass balance modeling independently of meteorological observations.

[59] 3. Projections of volume change in the 21st century driven by the B2 emission scenario from statistically downscaled RCA3 and six GCMs outputs result in a volume loss of 50–90% of the glacier's initial volume by end of 2100. Differences in these projections vary within 40% of the initial volume. Each volume projection varies within a range of 20% due to applied volume-area scaling or constant area. The choice of the method in the mass balance modeling, after excluding obvious outliers, corresponds to an uncertainty range of 10% for the volume projection, while the choice of the baseline period for the downscaling method results in 3% uncertainty range. In the range of uncertainties we need to add the uncertainty in the performance of the degree-day model itself: for the period of calibration 30% of the variance of the measured mass balance remains unexplained by the model. Modeled projections are not only highly sensitive to the choice of GCMs but can completely offset the results if seasonal biases in future series are not corrected by the reference climate, i.e., if a proper downscaling method is not applied.

[60] 4. The static mass balance sensitivities to future temperature and precipitation change, calculated as running difference between 20-year averages of b_n and averaged b_n over the reference period 2001–2020, show very small variations in time with the mean values of $db/dT = -0.48$ m yr^{-1} K^{-1} and $db/dP = 0.025$ m yr^{-1} per 1% precipitation increase.

[61] This sensitivity study showed that the model is capable of predicting future volume changes that are comparable with those derived from more sophisticated models [*Oerlemans et al.*, 1998; *Schneeberger et al.*, 2001] and that the estimated static mass balance sensitivity corresponds well to previous estimates on Storglaciären [*Braithwaite et al.*, 2002; *de Woul and Hock*, 2005]. A possible way of using our results for global assessment of glacier volume change in the 21st century is direct application of the model to other glaciated regions taking advantage of the model's simple data requirements available from ERA-40 reanalysis. However, further study is needed to evaluate how far the calibrated mass balance model for one glacier is transferable to other glaciers, and whether representative sets of model parameters can be found for glaciers in similar environmental settings. Alternatively, a more sophisticated mass balance model based on energy balance calculations [e.g., *Greuell and Konzelmann*, 1994] may be used, but it requires more inventory and climate data. In the end, one needs to find the balance between model requirements and data availability. At present, air temperature and precipitation are variables that are most readily available and have received most scrutiny in terms of validation and downscaling techniques, and are therefore the best suited for mass balance projections.

[62] **Acknowledgments.** This study is a contribution to the CE (Climate and Energy) project funded by Nordic Energy Research (NEFP). Financial support is provided by the Swedish Research Council for Environment, Agricultural Sciences and Spatial Planning, FORMAS (project 21.4/2003-0387). Gratitude is expressed to the Rossby Centrum at SMHI, particularly to E. Kjellström for providing the RCA3 data and P. Kållberg and C. Maass (ECMWF) for helping to retrieve ERA-40 data. The weather data and ERA-40 data were received from SMHI and ECMWF, respectively. Comments by C. Tijm-Reijmer, T. Jóhannesson, A. Arendt, an anonymous reviewer, R. Braithwaite, and scientific editor R. Anderson have helped to improve the paper.

References

Aðalgeirsdóttir, G., T. Jóhannesson, H. Björnsson, F. Pálsson, and O. Sigurðsson (2006), Response of Hofsjökull and southern Vatnajökull, Iceland, to climate change, *J. Geophys. Res.*, *111*, F03001, doi:10.1029/2005JF000388.

Arendt, A. A., K. A. Echelmeyer, W. D. Harrison, C. S. Lingle, and V. B. Valentine (2002), Rapid wastage of Alaska glaciers and their contribution to rising sea level, *Science*, *297*, 286–382.

Bahr, D. B., M. F. Meier, and S. D. Peckham (1997), The physical basis of glacier volume-area scaling, *J. Geophys. Res.*, *102*(B9), 20,355–20,362.

Braithwaite, R. J. (1984), Calculations of degree-days for glacier-climate research, *Z. Gletscherkd. Glazialgeol.*, *20*, 1–8.

Braithwaite, R. J., and Y. Zhang (1999), Modelling changes in glacier mass balance that may occur as a result of climate changes, *Geogr. Ann., Ser. A*, *81*(4), 489–496.

Braithwaite, R. J., Y. Zhang, and S. C. B. Raper (2002), Temperature sensitivity of the mass balance of mountain glaciers and ice caps as a climatological characteristic, *Z. Gletscherkd. Glazialgeol.*, *38*, 35–61.

Church, J. A., J. M. Gregory, P. Huybrechts, M. Kuhn, K. Lambeck, M. T. Nhuan, D. Qin, and P. L. Woodworth (2001), Changes in sea level, in *Climate Change 2001: The Scientific Basis*, edited by J. T. Houghton et al., pp. 639–693, Cambridge Univ. Press, New York.

de Woul, M., and R. Hock (2005), Static mass balance of Arctic glaciers and ice cap using a degree-day approach, *Ann. Glaciol.*, in press.

Dyurgerov, M. B., and M. F. Meier (2000), Twentieth century climate change: Evidence from small glaciers, *Proc. Natl. Acad. Sci. U. S. A.*, *97*(4), 1406–1411.

Elsberg, D. H., W. H. Harrison, K. A. Echelmeyer, and R. M. Krimmel (2001), Quantifying the effects of climate and surface change on glacier mass balance, *J. Glaciol.*, *47*(159), 649–658.

Giorgi, F., B. C. Hewitson, J. Christensen, M. Hulme, H. Von Storch, P. Whetton, R. L. Jones, L. Mearns, and C. Fu (2001), Regional climate information—Evaluation and projections, in *Climate Change 2001: The Scientific Basis*, edited by J. T. Houghton et al., pp. 583–638, Cambridge Univ. Press, New York.

Gregory, J. M., and J. Oerlemans (1998), Simulated future sea-level rise due to glacier melt based on regionally and seasonally resolved temperature changes, *Nature*, *391*, 474–476.

Greuell, W., and T. Konzelmann (1994), Numerical modelling of the energy balance and the englacial temperature of the Greenland ice sheet, Calculations for the ETH-camp location (west Greenland, 1155 m a.s.l.), *Global Planet. Change*, *9*(1–2), 91–114.

Hanna, E., P. Valdes, and J. McConnel (2001), Patterns and variations of snow accumulation over Greenland, 1979–98, from ECMWF analysis, and their verification, *J. Clim.*, *14*, 3521–3535.

Harrison, W. D., D. H. Elsberg, L. H. Cox, and R. S. March (2005), Different mass balance for climatic and hydrologic applications, *J. Glaciol.*, *51*(172), 176.

Hock, R. (2003), Temperature index melt modelling in mountain areas, *J. Hydrol.*, *282*(1–4), 104–115.

Hock, R., and B. Holmgren (1996), Some aspects of energy balance and ablation of Storglaciären, northern Sweden, *Geogr. Ann., Ser. A*, *78*(2–3), 121–131.

Hock, R., and B. Holmgren (2005), A distributed energy balance model for complex topography and its application to Storglaciären, Sweden, *J. Glaciol.*, *51*(172), 25–36.

Hock, R., P. Jansson, and L. Braun (2005), Modelling the response of mountain glacier discharge to climate warming, in *Global Change and Mountain Regions—A State of Knowledge Overview*, edited by U. M. Huber et al., pp. 243–252, Springer, New York.

Holmlund, P. (1987), Mass balance of Storglaciären during the 20th century, *Geogr. Ann., Ser. A*, *69*(3–4), 439–447.

Holmlund, P., P. Jansson, and R. Pettersson (2005), An analysis of mass changes of Storglaciären over the last 58 years, *Ann. Glaciol.*, in press.

Intergovernmental Panel on Climate Change (IPCC) (2001), *Climate Change 2001: The Scientific Basis. Contribution of Working Group 1 to the Third Assessment Report of the Intergovernmental Panel on Climate Change*, edited by J. T. Houghton et al., 881 pp., Cambridge Univ. Press, New York.

Kållberg, P. W., A. J. Simmons, S. M. Uppala, and M. Fuentes (2004), The ERA-40 archive, *ERA-40 Proj. Rep. Ser. 17*, 31 pp., Eur. Cent. for Medium-Range Weather Forecasts, Reading, U. K.

Kjellström, E., L. Bärring, S. Gollvik, U. Hansson, C. Jones, P. Samuelsson, M. Rummukainen, A. Ullerstig, U. Willén, and K. Wyser (2005), A 140-year simulation of European climate with the new version of the Rossby Centre regional atmospheric climate model (RCA3), *Rep. Meteorol. Climatol. 108,* Swed. Meteorol. and Hydrol. Inst., Norrköping.

Krenke, A. N., and V. G. Khodakov (1966), O svyazi poverkhnostnogo tayaniya ledinkov s temperaturoy vozdukha (The relationship between surface ice melting and air temperature), *Mater. Glyatsiol. Issled.*, *12*, 153–164.

Martin, E. (2004), Validation of Alpine snow in ERA-40, *ERA-40 Proj. Rep. Ser. 14*, 21 pp., Eur. Cent. for Medium-Range Weather Forecasts, Reading, U. K.

Meier, M., M. Dyurgerov, and G. J. McCabe (2003), The health of glaciers: Recent changes in glacier regime, *Clim. Change*, *59*(1–2), 123–135.

New, M., M. Hulme, and P. J. Jones (1999), Representing twentieth century space-time climatic variability, part 1: Development of a 1961–1990 mean monthly terrestrial climatology, *J. Clim.*, *12*, 829–856.

Oerlemans, J., et al. (1998), Modelling the response of glaciers to climate warming, *Clim. Dyn.*, *14*, 267–274.

Oerlemans, J., R. P. Bassford, W. Chapman, J. A. Dowdeswell, A. F. Glazovsky, J.-O. Hagen, K. Melvold, M. de Ruyter de Wildt, and R. S. W. van de Wal (2005), Estimating the contribution from Arctic glaciers to sea-level change in the next hundred years, *Ann. Glaciol.*, in press.

Pettersson, R., P. Jansson, and H. Blatter (2004), Spatial variability in water content at the cold-temperate transition surface of the polythermal Storglaciaren, Sweden, *J. Geophys. Res.*, *109*, F02009, doi:10.1029/2003JF000110.

Raper, S. C. B., and R. J. Braithwaite (2006), Low sea level rise projections from mountain glaciers and icecaps under global warming, *Nature*, *439*, 311–313, doi:10.1038/nature04448.

Rasmussen, L. A., and H. Conway (2004), Climate and glacier variability in western North America, *J. Clim.*, *17*(9), 1804–1815.

Reichert, B. K., L. Bengtsson, and J. Oerlemans (2001), Midlatitude forcing mechanisms for glacier mass balance investigated using general circulation models, *J. Clim.*, *14*(17), 3767–3784.

Salathé, E. P. (2005), Downscaling simulations of future global climate with application to hydrologic modelling, *Int. J. Climatol.*, *25*, 419–436.

Schneeberger, C., O. Albrecht, H. Blatter, M. Wild, and R. Hock (2001), Modelling the response of glaciers to a doubling in atmospheric CO_2: A case study of Storglaciären, northern Sweden, *Clim. Dyn.*, *17*, 825–834.

Simmons, A. J., and J. K. Gibson (2000), The ERA-40 project plan, *ERA-40 Proj. Rep. Ser. 1*, 63 pp., Eur. Cent. for Medium-Range Weather Forecasts, Reading, U. K.

Simmons, A. J., P. D. Jones, V. da Costa Bechtold, A. C. M. Beljaars, P. Kallberg, S. Saarinen, S. M. Uppala, P. Viterbo, and N. Wedi (2004), Comparison of trends and low-frequency variability in CRU, ERA-40, and NCEP/NCAR analyses of surface air temperature, *J. Geophys. Res.*, *109*, D24115, doi:10.1029/2004JD005306.

Vallon, M., C. Vincet, and L. Reynauld (1998), Altitudinal gradient of mass-balance sensitivity to climatic change from 18 years of observations on Glacier d'Argentière, France, *J. Glaciol.*, *44*(146), 93–96.

Van de Wal, R. S. W., and M. Wild (2001), Modelling the response of glaciers to climate change by applying volume-area scaling in combination with a high resolution GCM, *Clim. Dyn.*, *18*, 359–366.

Velicogna, I., J. Wahr, E. Hanna, and P. Huybrechts (2005), Short term mass variability in Greenland, from GRACE, *Geophys. Res. Lett.*, *32*, L05501, doi:10.1029/2004GL021948.

Widmann, M., C. S. Bretherton, and E. P. Salathé Jr. (2003), Statistical precipitation downscaling over the northwestern United States using numerically simulated precipitation as a predictor, *J. Clim.*, *16*, 799–816.

Wilby, R. L., T. M. L. Wigley, D. Conway, P. D. Jones, B. C. Hewitson, J. Main, and D. S. Wilks (1998), Statistical downscaling of general circulation model output: A comparison of methods, *Water Resour. Res.*, *34*, 2995–3008.

Xu, C.-Y. (1999), Climate change and hydrologic models: A review of existing gaps and recent research developments, *Water Resour. Manage.*, *13*, 369–382.

R. Hock and V. Radić, Department of Physical Geography and Quaternary Geology, Stockholm University, SE-10691 Stockholm, Sweden. (regine.hock@natgeo.su.se; valentina.radic@natgeo.su.se)